

## Structure of a 7Fe Ferredoxin from *Azotobacter vinelandii*\*

(Received for publication, October 20, 1980)

Debashis Ghosh, William Furey, Jr., Stephen O'Donnell, and Charles David Stout

From the Department of Crystallography, University of Pittsburgh, Pittsburgh, Pennsylvania 15260

The structure of the 7Fe ferredoxin from *Azotobacter vinelandii* has been solved from a 3.0-Å multiple isomorphous replacement map. The crystals belong to space group  $P4_32_12$  with  $a = 55.22$ ,  $c = 95.20$  Å, and  $Z = 1$ . Heavy-atom derivatives were prepared with  $K_2PtCl_4$ ,  $K_2[OsO_2(OH)_4]$ , and  $Na_3RhCl_6$ . Anomalous scattering data were collected for native (Fe) and Pt derivative crystals. The figure of merit for 3,322 reflections to 3.0 Å is 0.74.

The structure consists of an  $NH_2$ -terminal core of residues 1-50 which form the Fe-S cluster sites, and a  $COOH$ -terminal chain of residues 51-107 which wraps around this core. The [3Fe-3S] cluster is ligated by cysteines 8, 11, 16, 20, and 49 and a sixth ligand which is either glutamic acid 18 or an exogenous small molecule. The [4Fe-4S] cluster is ligated by cysteines 24, 39, 42, and 45. The coordination of both Fe-S centers has been confirmed by fitting of the cluster atoms and residues 1-50 to unbiased  $2F_o - F_c$  Fourier maps at 2.5-Å resolution. The structure of the 3Fe center has also been confirmed with anomalous scattering difference Fourier maps using both isomorphous replacement and refined phases. The partially refined structure at 2.5 Å (3,490 reflections, 6.0  $\sigma(|F|)$ ) has  $R = 35\%$ .

An iron-sulfur protein from *Azotobacter vinelandii* has been isolated and characterized (1-4) as containing two Fe-S centers per 14,000 daltons of molecular mass. EPR experiments demonstrated that the two clusters are both paramagnetic in their oxidized states in spite of the fact that the oxidation-reduction potentials are  $E_m = -0.424$  and  $+0.320$  V (5). This result established that a new type of Fe-S cluster was present, EPR-active in its oxidized state, and yet low potential in character. Displacement reactions have demonstrated the unique chemical nature of the cluster(s) present because of the nonstoichiometric yields of 2Fe and 4Fe centers and the unusual spectra obtained under extrusion conditions (6). Subsequently, Mössbauer experiments have shown that the low potential center is a new type of Fe-S cluster containing three iron atoms, while the high potential center is a 4Fe cluster with characteristics of the center in HiPIP<sup>1</sup> (7). Further

evidence for the presence of 3Fe centers in *Desulfovibrio gigas* ferredoxin II, aconitase, and glutamine synthase, very similar to the center in *Azotobacter* ferredoxin, has been obtained by Mössbauer spectroscopy (7, 8). This work has led to an electronic model for 3Fe centers (9).

A primary structure analysis of *Azotobacter* ferredoxin (10) revealed that the distribution of cysteines was nonhomologous with clostridial (8Fe) ferredoxin (11). The amino acid sequence of the entire molecule (107 residues) has been completed<sup>2</sup> and confirms this result.

X-ray crystallography was initiated with the objective of determining the structural features of this iron-sulfur protein responsible for its unique properties. Fe-S protein structures already solved are *Peptococcus aerogenes* 8Fe ferredoxin (12, 13), *Chromatium HiPIP* (14-16), *Spirulina platensis* 2Fe ferredoxin (17), and two rubredoxins (18, 19). Suitable crystals of *Azotobacter* ferredoxin were grown from  $(NH_4)_2SO_4$  using Tris buffer (20). At 4.0-Å resolution, it was apparent that the two clusters present in the molecule were distinctly different (21). At 2.5 Å, the resolution was sufficient to model the Fe-S electron density as [4Fe-4S] and [3Fe-3S] (22); the density for the new 3Fe structure proposed could not be interpreted in terms of known 4Fe and 2Fe structures. In this paper, the structures of the [3Fe-3S] and [4Fe-4S] clusters, their coordination by the protein, and the folding of the polypeptide chain are described. The model is derived from a 3.0-Å MIR map with partial refinement to 2.5-Å resolution. Iron atom positions have been confirmed with anomalous scattering and  $2F_o - F_c$  Fourier maps. The results confirm the proposed structure for the 3Fe center (22) and establish the conformation of a 7Fe ferredoxin.

### EXPERIMENTAL PROCEDURES

**Crystals**—Ferredoxin is purified by the method of Shethna (1) with modification (20). Cells have been obtained through the New England Enzyme Center and as gifts from Dr. W. J. Brill (University of Wisconsin, Madison) and Dr. W. V. Sweeney (Hunter College, New York). In all cases, the organism cultured has been *A. vinelandii* OP (ATCC No. 13705). Yields of ferredoxin are 5-10 mg/kg of cells with a purity index  $A_{280}/A_{400}$  in the range of 1.64-1.80.

Tetragonal crystals are grown using a temperature gradient and Tris buffer (20). The space group is  $P4_32_12$  with  $a = 55.22$ ,  $c = 95.20$  Å and one molecule per asymmetric unit. Diffraction patterns extend isotropically to 2.0-Å resolution.

Tetragonal crystals have been obtained in all 27 preparations done to date. Crystals have also been grown from cell extracts prepared by osmotic shock in the absence of butanol (nitrogenase extracts). Further, triclinic crystals (20) have been grown as an assay for purity in all preparations. These crystals have the same appearance as those obtained by Yoch and Arnon (3) and display diffraction patterns identical to those recorded from triclinic crystals originally obtained by Sieker *et al.*<sup>3</sup> At the same time, diffraction patterns for all tetra-

\* This research is supported by National Institutes of Health Grant GM-25672. The MMS-X graphics facility was developed through a grant from the Division of Research Resources, National Institutes of Health, to the Computer Systems Laboratory, Washington University, St. Louis, Missouri. The costs of publication of this article were defrayed in part by the payment of page charges. This article must therefore be hereby marked "advertisement" in accordance with 18 U.S.C. Section 1734 solely to indicate this fact.

<sup>1</sup> The abbreviations used are: HiPIP, high potential iron protein; MIR, multiple isomorphous replacement; SIR, single isomorphous replacement;  $R$ ,  $\Sigma ||F_o| - k|F_c|| / \Sigma |F_o|$  where  $|F_o|$  and  $|F_c|$  are observed and calculated native structure amplitudes, respectively; A, alanine; F, phenylalanine; G, glycine; E, glutamic acid; Y, tyrosine; H, histidine; W, tryptophan; K, lysine; R, arginine; M, methionine; L, leucine; P, proline; D, aspartic acid; N, asparagine; C, cysteine; V,

valine; I, isoleucine; T, threonine; X, variable; S, serine; Lx, uncharacterized ligand.

<sup>2</sup> T. Lorschach, J. B. Howard, K. Melis, and C. D. Stout, manuscript in preparation.

<sup>3</sup> L. C. Sieker, Y. I. Shethna, C. D. Stout, and M. Sundaralingam (1970) unpublished results.

gonal crystals obtained from different preparations are identical. Therefore, the crystallization of this protein does not appear to be an artifact, and one must conclude that the molecule as isolated and studied under a variety of conditions is the same as the molecule that crystallizes.

**Data Collection**—Native and derivative data used in the final phase determination are listed in Table I. Data were collected with a Picker FACS-1 diffractometer using programs developed by Dr. R. McClure (University of Pittsburgh). Details of the data collection scheme and scaling procedure for Os and Rh derivative data were the same as already described for native and Pt derivative data (22).

**Heavy Atom Derivatives**—Heavy atom derivatives were prepared by soaking the crystals in their mother liquor, or in a stabilizing solution chosen to optimize heavy atom binding (Table II). Derivatives were screened at 2°C using the precession camera and promising candidates were further examined on the diffractometer until intensity differences could be reproduced. Of over 80 reagents screened in this manner, only those listed in Table II were found to bind isomorphously. Two compounds,  $K_2PdCl_4$  and  $K_2RuCl_6$ , caused large non-isomorphous changes; thiol specific reagents such as  $KAuCl_4$  or  $HgCl_2$  reacted directly with the Fe-S centers to decolor and denature the crystals; all of the remaining reagents used had no effect whatsoever on the native diffraction pattern. This was true even under extreme conditions, e.g. saturated  $SmCl_3$  soaked for two weeks at 37°C. Isomorphous derivative crystals displayed changes in the *c* axis direction of up to 1.0 Å.

**Phase Calculations**—The single major Pt site was located from isomorphous and anomalous difference Patterson maps (Fig. 1). Protein phases calculated from this derivative in conjunction with anomalous scattering data from both the native (Fe) and derivative (Pt + Fe) crystals were used to determine the space-group and heavy atom absolute configuration (21). Four protein phase sets were derived using the Pt data without anomalous dispersion, for space groups  $P4_32_12$  and  $P4_32_12$ , and with Pt at both  $(x,y,z)$  and  $(\bar{x},\bar{y},\bar{z})$ . Only one phase set ( $P4_32_12$ ,  $\bar{x},\bar{y},\bar{z}$ ) gave large positive peaks at the two Fe-S cluster sites in both the native "best" Fourier and the "Bijvoet difference" (23) Fourier maps (Figs. 2 and 3).

The Os and Rh derivatives were solved by difference Fourier methods and confirmed with isomorphous difference Patterson maps. Protein phases and heavy atom sites determined by pair-wise combination of the derivatives yielded mutually consistent cross-difference Fourier maps for all three combinations (24). A second Pt derivative with somewhat different substitution was prepared by first exchanging the mother liquor for 90% saturated potassium phosphate, pH 7.4 (Table II) (25). Minor sites in all the derivatives were located from difference difference maps. The heavy atom parameters and isomorphous replacement protein phases were then refined using the program of M. G. Rossmann (Purdue University)<sup>4</sup> (26) with inclusion of the anomalous scattering data for the Pt-sulfate derivative. Each derivative crystal was refined separately in order to allow for differences in soaking conditions. Final heavy atom parameters are listed in Table III.

**Electron Density Maps**—Two electron density maps have been calculated: at 2.5-Å resolution for study of the Fe-S clusters and at 3.0-Å resolution for chain tracing and model building. The 2.5-Å map is based on isomorphous and anomalous data from the two Pt derivatives alone (SIR map) and has an overall figure of merit of 0.61 for 5249 reflections (22). The 3.0-Å map is based on all the derivatives (MIR map) and has an overall figure of merit of 0.74 for 3322 reflections.

**Model Building and Refinement**—The 3.0-Å MIR map and the 2.5-Å SIR map were studied on a scale of 1.0 cm/Å for chain tracing. The initial model was built into the MIR density using the departmental MMS-X interactive graphics facility and the BUILD system of programs (48).<sup>5</sup> The  $NH_2$ -terminal amino acid sequence from *Azotobacter* (10) and the complete sequence of the homologous protein from *Pseudomonas ovalis* (27) were used in the initial interpretation. Subsequently, the complete *Azotobacter* sequence<sup>2</sup> has been used. Coordinates of the starting model (876 atoms) were refined using the restrained-constrained least squares method of Konnert (28) and a computer program of W. Hendrickson (Naval Research Laboratory, Washington, D. C.) implemented by one of us (W. F.) on

TABLE I  
Data-collection summary

Data	No. of crystals	Resolution Å	Total reflections	Independent reflections	$RF^a$ %
Native	7	2.5	18,117 <sup>b</sup>	5,236	
Pt-sulfate	7	2.5	20,019 <sup>b</sup>	5,606	16
Pt-phosphate	1	4.0	1,518	1,455	21
Os	2	3.0	6,808	3,070	21
Rh	1	3.0	3,508	3,332	25

<sup>a</sup>  $RF = \sum |k|F_{PH}| - |F_P| / \sum |F_P|$ .  $|F_P|$ ,  $|F_{PH}|$ , native and derivative structure amplitudes, respectively; *k*, scale factor for derivative data.

<sup>b</sup> Includes Bijvoet pair reflections.

the University DEC-10 and FPS 190L array processor (29). After 15 cycles, the *R* factor was 35% for 3490 reflections ( $|F| \geq 6.0 \sigma(|F|)$ ) in the range 5.0–2.5 Å. The root mean square shift for all atoms was 1.128 Å and the root mean square deviation from ideal bond lengths was 0.039 Å. Unbiased  $2F_o - F_c$  Fourier maps to 2.5 Å, prepared by omitting 7–10 residues from the phase calculation, have been used to monitor the refinement and for refitting of the protein model at 2.5-Å resolution. Details of the refinement will be presented elsewhere.

## RESULTS

**Protein Folding**—The folding of the polypeptide chain and the manner in which the Fe-S clusters are ligated was deduced from the 3.0-Å MIR map. Sections of the electron density map and the fitted model are shown in Fig. 4. A schematic drawing of the structure is shown in Fig. 5. The coordination of Fe-S clusters with respect to the amino acid sequence is depicted in Fig. 6. The connectivity of the polypeptide backbone electron density is unbroken throughout the entire chain, except at the  $NH_2$  terminus between A1 and F2, and at G28, where the chain makes a sharp turn at the surface of the molecule. The nine cysteines, the methionine, and all 20 proline and aromatic residues have electron densities for their side chains in accord with the sequence (10).<sup>2</sup> Improved  $2F_o - F_c$  maps at 2.5 Å have confirmed these side chain assignments and have brought up the missing density at A1 and G28.

The structure may be described in two segments: an  $NH_2$ -terminal core of residues 1–50 which enfolds the Fe-S clusters, followed by a  $COOH$ -terminal chain of residues 51–107 which wraps around this core. The  $NH_2$ -terminal portion may be subdivided into residues 1–20, which create the 3Fe center-binding cavity, and residues 21–50 which incorporate the 4Fe center. The structure consists almost entirely of extended chains and sharp turns. The polar side chains all lie at the surface of the molecule with the notable exception of E18. The majority of the hydrophobic side chains are either close-packed in the interior of the molecule or in association at the surface. Surprisingly, 9 of the 11 aromatic residues are either fully or partially exposed to solvent, and 6 lie across the one side of the molecule in a 30-Å belt: F2, F25, Y26, F31, H35, and W78. There is a marked clustering of basic residues in the vicinity of the 3Fe center: K10, K12, K98, K100, H103, and R106.

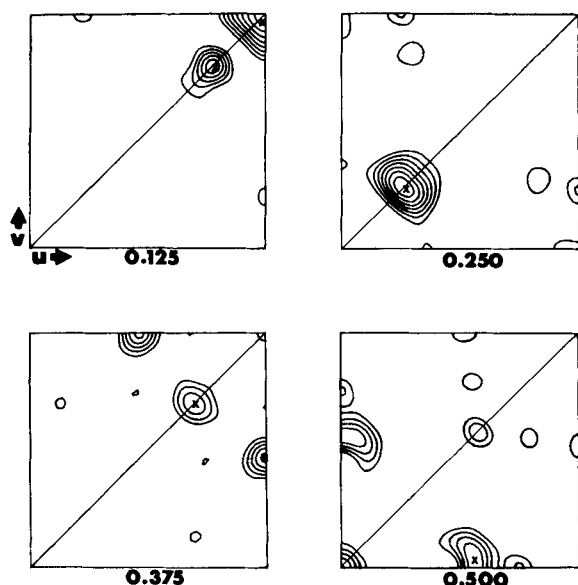
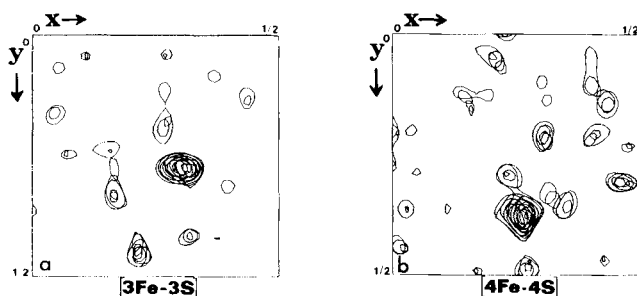
In the present model, residues 1–107 and the [3Fe-3S] and [4Fe-4S] clusters have been fit to the MIR density and refined 15 cycles to *R* = 35%. Subsequently, residues 1–50 and all atoms of both clusters have been fit to unbiased  $2F_o - F_c$  maps at 2.5 Å using the refined phases in order to confirm the ligand assignments and the structure of each cluster. Fitting of residues 51–107 to  $2F_o - F_c$  maps is in progress. A complete description of the intra- and intermolecular interactions and hydrogen bonding, the solvent structure, and details of the Fe and S stereochemistry (root mean square  $\Delta d < 0.2$  Å) requires further refinement of the model. Coordinates of the current

<sup>4</sup> M. G. Rossmann, Heavy Atom Least Squares Refinement Program.

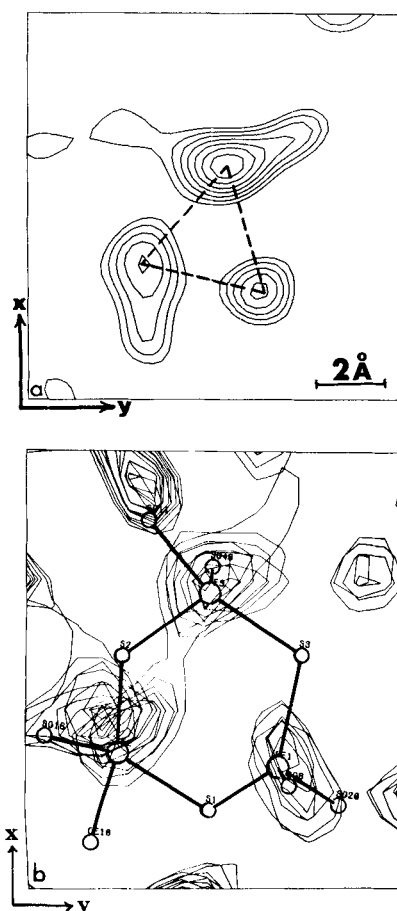
<sup>5</sup> J. P. McAlister, and C. D. Barry, Computer Systems Laboratory, Washington University, St. Louis, Mo., Protein Model Building and Density Fitting Programs.

TABLE II  
Heavy atom derivatives

Derivative	Compound	Soaking solution	Concentration	Time	Temperature
			<i>mM</i>		$^{\circ}\text{C}$
Pt-sulfate	$\text{K}_2\text{PtCl}_4$	3.5 M $(\text{NH}_4)_2\text{SO}_4$ 0.5 M Tris-HCl (pH 7.6)	2 <sup>a</sup>	4 days	2
Pt-phosphate	$\text{K}_2\text{PtCl}_4$	4.8 M $\text{K}_2\text{HPO}_4/\text{KH}_2\text{PO}_4$ (pH 7.4)	$\sim 10^a$	6 days	2
Os	$\text{K}_2[\text{OsO}_2(\text{OH})_4] \cdot 2\text{H}_2\text{O}$	4.5 M $(\text{NH}_4)_2\text{SO}_4$ 1.0 M $\text{K}_2\text{HPO}_4/\text{KH}_2\text{PO}_4$ (pH 5.2)	Saturated	3 weeks	2
Rh	$\text{Na}_3\text{RhCl}_6 \cdot 18\text{H}_2\text{O}$	4.5 M $(\text{NH}_4)_2\text{SO}_4$ 1.0 M Tris-maleate (pH 6.4)	10	1 week	22

<sup>a</sup> Fresh solutions of  $\text{K}_2\text{PtCl}_4$  were soaked in the dark.FIG. 1. Isomorphous difference Patterson map for  $\text{PtCl}_4^{2-}$ -sulfate derivative. Mirror plane along  $[110]$  direction, sections on  $W$ , Harker sections at 0.250, 0.500. A single major binding site at  $(x,y,z) = (0.481, 0.135, 0.315)$  gives rise to the six independent vectors marked.FIG. 2. Bijvoet difference (anomalous scattering) Fourier map at 4.0-Å resolution. Computed with MIR phases for 969 acentric reflections. Composite sections on  $z = 0.27$ – $0.29$  for 3Fe center (a); 0.37–0.39 for 4Fe center (b).model have been submitted to the Protein Data Bank.<sup>6</sup>

**Fe-S Sites**— The two Fe-S clusters are separated by 12 Å (minimum distance, 9 Å edge to edge) and both lie relatively near the “upper” surface of the molecule (view in Fig. 5). In other words, the clusters are displaced from the center of gravity of the protein. Conversely, the COOH-terminal 57 residues wrap around all but the upper side of the  $\text{NH}_2$ -

FIG. 3. Bijvoet difference Fourier maps at 2.5-Å resolution. a, map for the 3Fe center at 2.5 Å, calculated with SIR phases (2267 acentric reflections). Section at  $z = 0.28$ . b, map for the  $[3\text{Fe}-3\text{S}]$  cluster at 2.5 Å, calculated with phases from the protein model after 15 cycles of refinement ( $R = 35\%$ ) (the same 2267 coefficients as in a). All atoms of the cluster and ligand amino acids were omitted from the phase calculation. Composite sections on  $z: 0.265$ – $0.295$ . Peaks at the edges of the map arise from other protein residues input in the phase calculation which bias the difference Fourier map.

terminal core. In so doing, this chain forms a cleft below the 3Fe center (residues E66–P79 on the “left,” Fig. 5; and D90–G99 on the right). The intervening segment, N80–P89, forms a large, open loop, which is packed about a 2-fold axis in the crystal. The accessibility of each cluster to solvent is consistent with what one would expect on the basis of their respective potentials. The low potential 3Fe center ( $E_m = -0.424$  V), although ligated at six points, is relatively exposed to solvent due to the cleft and the openness of the C11–C16 loop, while

<sup>6</sup> F. C. Bernstein, Chemistry Department, Brookhaven National Laboratory, Upton, New York 11973.

TABLE III  
Heavy atom parameters

Derivative	Site	$A^a$	$x$	$y$	$z$	$B^b$	$f_H/E^c$
Pt-sulfate	1	67.26	0.4811	0.1347	0.3150	27.29	2.29
	2	4.54	0.4509	0.2026	0.1759	5.00	
	3	4.97	0.2633	0.3088	0.2972	5.00	
Pt-phosphate	1	107.25	0.4671	0.1245	0.3211	36.28	2.26
	2	11.15	0.4613	0.1806	0.1810	5.00	
	3	14.13	0.2747	0.2981	0.2953	5.00	
	4	12.54	0.0467	0.2096	0.5024	38.79	
	5	9.33	0.2052	0.1159	0.3456	11.76	
	6	8.20	0.3880	0.2135	0.1813	5.00	
	7	6.30	0.4185	0.2471	0.4749	7.52	
Os	1	74.75	0.1017	0.2104	0.4425	29.14	1.14
	2	54.84	0.4720	0.0835	0.4771	9.16	
	3	60.46	0.3161	0.2553	0.2822	8.45	
	4	17.99	0.3362	0.1213	0.4183	5.00	
	5	11.62	0.2378	0.3690	0.3796	16.67	
	6	18.00	0.2588	0.2900	0.3028	5.00	
Rh	1	40.54	0.4787	0.1280	0.3256	9.61	1.20
	2	29.91	0.1130	0.2111	0.4504	8.62	
	3	8.05	0.3330	0.4009	0.1140	5.00	
	4	24.86	0.3098	0.2603	0.2830	5.00	
	5	12.51	0.1352	0.4397	0.4615	5.00	
	6	14.83	0.4583	0.1039	0.4771	17.59	
	7	7.56	0.0582	0.4011	0.3562	5.00	
	8	4.35	0.1802	0.4422	0.1194	6.97	
	9	12.90	0.4227	0.2424	0.3121	5.00	
	10	11.21	0.2641	0.3770	0.3799	15.12	
	11	15.55	0.2607	0.2895	0.3027	5.00	
	12	7.73	0.1829	0.2758	0.1995	5.00	

<sup>a</sup> Occupancy relative to an arbitrary scale of  $|F_P| \times 20.00$ .  $|F_P|$ , native structure amplitude. A Wilson plot of the native data,  $|F_P|$ , to 2.5 Å, yields a scale of 18.36.

<sup>b</sup> Shape parameter, Å<sup>2</sup>. When  $B$  refined to a value less than 5.00,  $B$  was arbitrarily fixed at 5.00.

<sup>c</sup>  $f_H$ , average heavy atom structure amplitude;  $E$ , average lack of closure error.

the high potential 4Fe center ( $E_m = +0.320$  V) is surrounded by close-packed hydrophobic side chains.

**[3Fe-3S] Cluster**—The arrangement of the Fe, S, and  $S_\gamma$  atoms in the 3Fe center is shown in Fig. 7a. The three Fe atoms of the cluster are bound to the protein by the  $S_\gamma$  atoms of cysteines 8, 11, 16, 20, and 49. A sixth ligand,  $L_x$ , must be either the side chain of E18 or an exogenous small molecule. Positions of the atoms have been derived by three independent means: by fitting both the cluster and amino acid sequence to the MIR map, by fitting residues 1–50 and then the cluster and ligand atoms to unbiased  $2F_o - F_c$  maps, and by calculating Bijvoet difference (anomalous scattering) Fourier maps with SIR and refined protein phases (Fig. 3). The bond distances and angles are within the ranges commonly observed for Fe, S, and  $S_\gamma$  atoms, and the Fe atoms have essentially tetrahedral geometry. In the present model, the Fe-Fe distances are: Fe1-Fe2, 4.2 Å; Fe1-Fe3, 4.4 Å; Fe2-Fe3, 4.1 Å.

One potentially useful way in which to describe the geometry of the 3Fe center is as a dimer with insertion of a  $FeS_2(S_\gamma)(L_x)$  moiety, and this description may have chemical significance as well. In the view of Fig. 7a, the inorganic sulfur atom S3 is in the plane defined by the three Fe atoms. In addition, iron atoms Fe1 and Fe3 have only  $S_\gamma$  ligands:  $S_\gamma 8$  above the plane,  $S_\gamma 20$  below the plane on Fe1;  $S_\gamma 11$  above the plane,  $S_\gamma 49$  below the plane on Fe3. This grouping of atoms,  $[2Fe-S](S_\gamma)_4$  (dotted line, Fig. 7a), is therefore similar to the structure of the  $[2Fe-2S](S_\gamma)_4$  cluster in *S. platensis* ferredoxin (17), a planar "core" (Fe1, Fe3, S3) with  $S_\gamma$  ligands at right

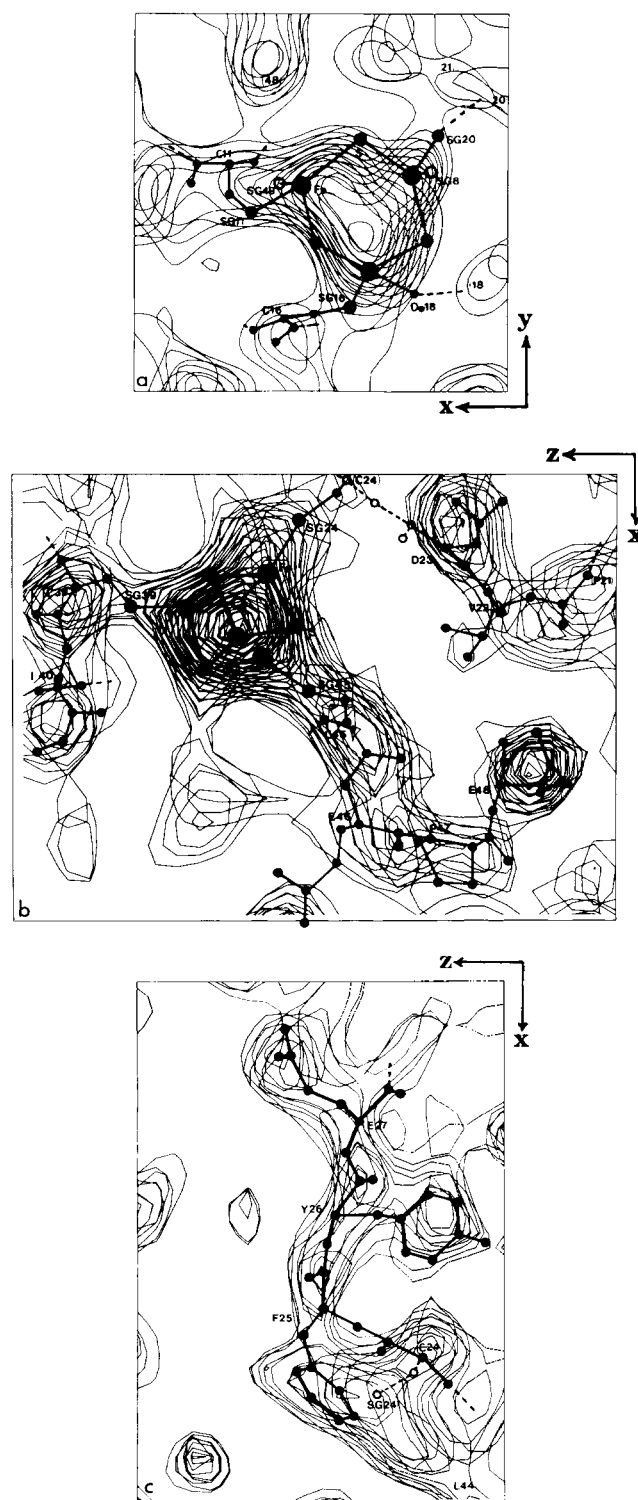


FIG. 4. 3-Å MIR map and coordinates of protein model. *a*, composite sections on  $z$ : 0.265–0.295 enclosing the [3Fe-3S] cluster. The trilobal nature of the cluster density is apparent. All of the atoms of residues 8 and 49 are above and below, respectively, the sections shown, and most of the atoms of residues 18 and 20 are below the sections. *b*, composite sections on  $y$ : 0.360–0.430 enclosing the [4Fe-4S] cluster and three adjacent segments of the protein chain. Same view as in Fig. 5. Cysteine 42 attaches to the cluster from above the sections shown; one inorganic S atom is below. Density between I40 and E46 adjacent to the cluster belongs to S56. *c*, composite sections on  $y$ : 0.450–0.500 showing residues 24–27 and adjacent solvent channel. Same orientation as in *b* (and Fig. 5), with superposition at C24. F25 stacks on the 4Fe center.

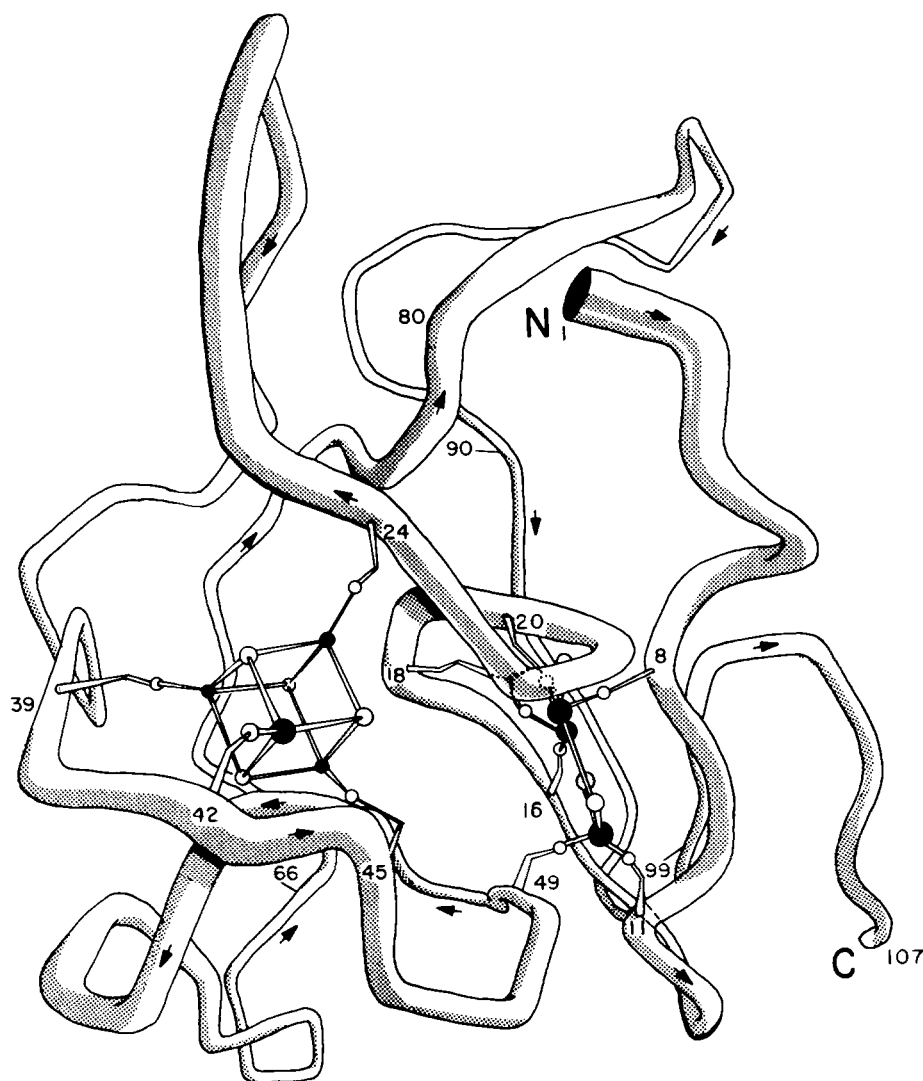


FIG. 5. The structure of *Azotobacter ferredoxin* showing the course of the polypeptide chain, the Fe-S clusters, ligand residues, and selected residue numbers. Drawing based on  $C_{\alpha}$  coordinates; view is down  $+y$  direction. As shown, the E18 side chain is a ligand to the  $[3\text{Fe}\cdot 3\text{S}]$  cluster, although this feature of the structure is not firmly established (see text).

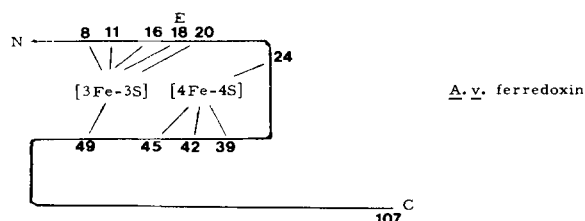


FIG. 6. Ligation of the two Fe-S clusters with respect to the amino acid sequence (after Adman, *et al.* (12). Numbers, cysteine residues; E18, glutamic acid residue 18; A. v., *A. vinelandii*).

angles to the plane of the dimer fragment. The Fe atom "inserted" by replacement of an inorganic S atom with  $\text{FeS}_2(\text{S}_\gamma)(\text{L}_\alpha)$  is also the Fe atom (Fe2) with the non-cysteinylligand. The insertion alters the geometry considerably, however; the Fe1-Fe3 distance is approximately 1.7 Å greater than in the dimer (2.7 Å) (30).

A consistent view of the 3Fe center is to describe its conformation as a twist-boat. By placing S3 in the plane of the iron atoms, S1 is puckered significantly below the plane and the Fe atoms are oriented so as to make tetrahedral coordination with all six ligand atoms. (In the present model, S2 is in, rather than above, the plane of the cluster, as would be expected for an ideal twist-boat.) The  $[3\text{Fe}\cdot 3\text{S}]$  cluster is like the structure of an analog compound,  $[(\text{CH}_3)_2\text{SnS}]_3$ , where the Sn-Sn distances are 3.8 Å (31). In that case, a twist-boat

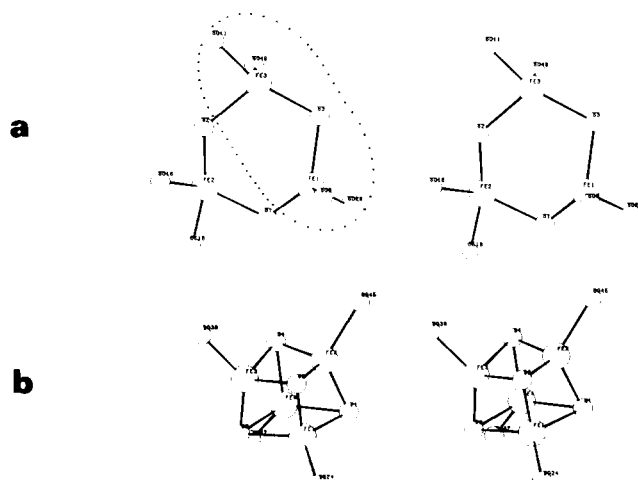


FIG. 7. Geometry of the  $[3\text{Fe}\cdot 3\text{S}]$  (a) and  $[4\text{Fe}\cdot 4\text{S}]$  (b) clusters. Atomic positions are derived from fitting unbiased  $2F_o - F_c$  Fourier maps at 2.5-Å resolution. Geometry has not been idealized. The sixth, non-cysteinylligand of the  $[3\text{Fe}\cdot 3\text{S}]$  cluster is denoted as the  $\text{O}_{\epsilon 1}$  atom of the E18 side chain.

conformation minimizes van der Waals contacts between S and  $\text{CH}_3$  groups.

**[4Fe-4S] Cluster**—The four Fe atoms are bonded to the protein by the S atoms of cysteines 24, 39, 42, and 45 (Fig.

7b). The positions of the cluster and ligand atoms have been derived from the MIR and  $2F_o - F_c$  maps just as for the 3Fe center. The unrefined cluster has a structure very like the [4Fe-4S] clusters in the HiPIP (16), *P. aerogenes* ferredoxin (13) and analog complexes (30) with Fe-Fe distances of 2.7 Å. As all the data collection has been done with protein isolated and crystallized in air, the 4Fe HiPIP-like center should be in the reduced, or "C" oxidation state due to the presence of the low potential 3Fe center, unless the cluster has been oxidized by the x-ray beam (15).

**Anomalous Scattering Data**—Bijvoet difference Fourier maps have been calculated as an independent check of the Fe positions. At 4.0-Å resolution (Fig. 2), the two highest peaks in the asymmetric unit correspond to the Fe-S centers in the native structure. Essentially the same map is obtained with data from a second native crystal and with data from the Pt-sulfate derivative crystal for Bijvoet pairs collected as  $hkl/khl$  or  $hkl/\bar{h}\bar{k}\bar{l}$ . Moreover, the peak shapes are consistent with the two cluster structures.

At 2.5 Å, the individual Fe atoms of the 3Fe center are resolved in Bijvoet difference Fourier maps based on SIR phases (Fig. 3a) or phases calculated from the protein model (Fig. 3b). The Fe atoms of the 4Fe cluster, however, being at least 1 Å nearer each other, are not resolved at this resolution. Also, with the quality of the data available, it is not possible to clearly distinguish sulfur atoms from the noise level ( $f''_S = 1.1 e^-$  versus  $f''_{Fe} = 3.4 e^-$  for CuK  $\alpha$  radiation). Nevertheless, all four of the S<sub>i</sub> atoms about the 4Fe cluster have discernible peaks in the 4-Å Bijvoet-difference map (Fig. 2b and y-axis projection) whereas there are no S<sub>i</sub> peaks near the 3Fe center. An explanation for this may be an observation made by Kraut regarding the anomalous scattering from HiPIP (32). For that 4Fe center the majority of large Bijvoet differences occurred at less than 5-Å resolution in keeping with the Fourier transform (structure factor) of a tetrahedral object (33). For *Azotobacter* ferredoxin, the use of lower resolution (4 Å) data would be expected to enhance the appearance of the tetrahedral 4Fe cluster over the asymmetric 3Fe cluster. In retrospect, this effect could also explain the underweighting of the 3Fe center real electron density at 4-Å resolution (21).

**Heavy-atom Binding**—Under the soaking conditions used (Table II), the metal complexes probably involved in binding to ferredoxin are  $[PtCl_4]^{2-}$ ,  $[OsO_2(NH_3)_4]^{2+}$  and  $[Rh(NH_3)_nCl_m]^{(n-3-m)+}$  ( $m + n = 6$ ). The anionic Pt and cationic Os complexes have mutually exclusive major binding sites. The Rh derivative has predominant sites in common with both derivatives, perhaps due to the range of charged species which can be formed.

Of particular interest are two binding sites at the 3Fe center which indicate some degree of conformational change within this region of the molecule. The Os3 and Rh4 sites (Table III) occur at 0.31, 0.26, 0.28, or about 1.8 Å and 3.4 Å from Fe3 and Fe1, respectively (Fig. 7a), near the center of the cluster. The cationic amine complex may be able to make  $NH \cdots S$  hydrogen bonds (41) to the cluster. A secondary site at 0.26, 0.29, 0.30 for all the derivatives (Pt3, Os6, Rh11) is adjacent to S<sub>7</sub>, 20 and S1 (2.2 Å and 1.8 Å from these atoms, respectively).

The single major Pt site occurs at methionine 64. Apparently,  $[PtCl_4]^{2-}$  is excluded from the electronegative Fe-S sites and is able to react only with methionine sulfur. However, in so doing, the M64 side chain must be displaced from its position in the native structure, since the MIR map contains a large spurious peak at the Pt site. The conformational change would give rise to local nonisomorphism and hence a scaling error. Isomorphous replacement phases calculated with the Pt1 and Rh1 sites excluded lead to an electron

density map which shows the M64 side chain with the S<sub>8</sub> atom located exactly at the Pt site.

## DISCUSSION

**The 3Fe Peptide: CVEVCP**—The protein structure may be thought of as comprising bidentate and tridentate peptide ligands. In these terms, the sequence forming the 3Fe center is particularly striking. It consists of C<sub>8</sub>IKC<sub>11</sub>, a loop of four residues (K<sub>12</sub>YTD<sub>15</sub>), and the "3Fe peptide," C<sub>16</sub>VE<sub>18</sub>VC<sub>20</sub>P, which provides two cysteinyl ligands to the [3Fe-3S] cluster and then turns the chain toward the 4-Fe center. The sequence CVEVCP appears to be a special requirement for the formation of a [3Fe-3S] cluster. In this 7Fe, 9 cysteine-containing ferredoxin glutamate 18 could act as the tenth required ligand. In this case, the C<sub>16</sub>VE<sub>18</sub> tripeptide coordinates the same iron (Fe2, Fig. 7a); the E<sub>18</sub>VC<sub>20</sub> tripeptide coordinates two different irons (Fe2, Fe1) ~4 Å apart. This demonstrates the potential flexibility of glutamate in forming different chelate structures inherent in the longer side chain (five single bonds between C<sub>α</sub> and Fe compared to three between C<sub>α</sub> of cysteine and Fe). This peptide sequence also shows that only one intervening residue is required in each instance between glutamate and cysteine.

The sequence CVEVCP, or a closely homologous sequence, is found in at least six other ferredoxins whose properties suggest the presence of 3Fe centers. The organisms in which the ferredoxins are found and the peptide sequences are: *Pseudomonas ovalis* (27), CVEVCP; *Chromatium* (34, 35), CVEVCP; *Thermus thermophilus*,<sup>7</sup> CVEVCP; *Desulfovibrio gigas* (36), CVEICP; *Desulfovibrio africanus* (37), CVEICP; and *Mycobacterium smegmatis* (38), CIEECP. The *D. gigas* ferredoxin II protein has already been shown by Mössbauer spectroscopy to be a 3Fe protein, and is particularly interesting because of the 4Fe center, ferredoxin I state of the same polypeptide (8). The *Chromatium* protein is interesting because two reduced-state, EPR-active centers are present (39). The *T. thermophilus* protein, on the other hand, apparently has a low potential 4Fe center in conjunction with an *Azotobacter*-type 3Fe center (40). The *M. smegmatis* ferredoxin has a sequence change in the NH<sub>2</sub> terminus suggesting that C<sub>8</sub>VD<sub>10</sub>V is substituting for C<sub>8</sub>IKC<sub>11</sub> of the *Azotobacter* 3Fe center. In view of this diversity of properties it cannot be assumed that these ferredoxins all possess [3Fe-3S] clusters. Nevertheless, the prevalence of a CVEVCP type of sequence indicates its versatility in the formation of Fe-S centers. Correlation of the sequence data with the complete *Azotobacter* ferredoxin sequence and structure will be presented elsewhere.

**The 3Fe Center**—The coordination in this cluster bears a relation to the 2Fe center in *S. platensis* ferredoxin (17). In that protein, the ligand residues are C41, C46 to one Fe atom, and C49, C79 to the second, or cysteines  $n$ ,  $n + 5$ ,  $n + 8$ , and  $n'$ . Considering the 3Fe center as a dimer fragment with FeS<sub>2</sub>(S<sub>γ</sub>)(L<sub>x</sub>) inserted, the "dimer" in *Azotobacter* is coordinated by cysteines 8, 11, 20, 49 or  $n$ ,  $n + 3$ ,  $n + 12$ ,  $n'$ . Thus, both structures have a CXXC ( $n$ ,  $n + 3$ ) sequence which binds to separate Fe atoms of the dimer. The prevalence of CXXC sequences in 1Fe and 4Fe proteins has been discussed in terms of the  $NH \cdots S_{\gamma}$  hydrogen bonds which are formed (41). In the 3Fe center, each of the first three cysteines in the sequence, C8, C11, and C16, binds to a different Fe atom.

Mössbauer spectra of reduced *Azotobacter* and *D. gigas* ferredoxin exhibit a 2:1 ratio of Fe species for the 3Fe center as  $2Fe^{2.5+}/1Fe^{3+}$  (7-9). It seems plausible that there is a

<sup>7</sup> S. Sato, K. Nakazawa, K. Hon-nami, and T. Oshima, (1980) unpublished results, communicated by T. Ohnishi.

correlation between this ratio and the structure of the cluster, since the non-cysteinylligand on Fe2 (Fig. 7a) may stabilize a ferric ion. The greater Fe-Fe distances in this cluster might also allow greater localization of charge on a given Fe atom. In any case, the results imply that in *D. gigas* the 3Fe center has a non-cysteinylligand like the *Azotobacter* cluster, even though six cysteines are present (36).

Displacement reactions with *Azotobacter* ferredoxin give nonstoichiometric yields of 2Fe and 4Fe centers upon extrusion of the clusters with *o*-xylyldithiol or thiophenol (6). It has been pointed out that under these conditions the 3Fe center decomposes to a [2Fe-2S] cluster (7). The rearrangement could involve the dimer fragment embedded in the  $S_\gamma$  atoms of cysteines 8, 11, 20, and 49. A 2Fe center is also extruded from the 3Fe center in aconitase, but all of the Fe in the native enzyme is recovered as [2Fe-2S] clusters (42), suggesting a dismutation of the six-atom [3Fe-3S] ring rather than a fragmentation.

In addition to the Mössbauer evidence for 3Fe centers in aconitase and glutamine synthase (7), the electronic properties of ferredoxins from *Rhodospirillum rubrum* (43), *Corynebacterium autotrophicum* (44), *Mycobacterium flavum*, (45) and *Spirillum lipoferum* (45) suggest that these proteins contain 3Fe centers as well. It appears, therefore, that 3Fe centers may be as widespread in biological systems as 1Fe, 2Fe and 4Fe centers. In contrast to these, however, one might expect the open, six-member ring of the 3Fe center, especially when liganded by a glutamate side chain, to be conformationally quite flexible. Hence, 3Fe centers may be able to exist in a variety of states depending upon the protein environment.

**Molecular Conformation.**—The 3Fe center binding cavity is created by a run of four cysteines (8, 11, 16, 20) plus one from a distal portion of the sequence (residue 49). The 4Fe center is formed from a triplet of cysteines (residues 39, 42, 45) plus one cysteine (residue 24) distal in the sequence. This arrangement preserves the overall similarity of cluster coordination in this molecule with that in *P. aerogenes* ferredoxin (12) (Fig. 6). This is especially evident for the portion of the structure involving residues 20–50. Both the peptides  $C_{20}PV$  and  $C_{49}PA$  direct the chain away from a Fe-S cluster as in the *P. aerogenes* structure. The linking peptide  $C_{45}EPEC_{49}$  serves the same role as  $C_{41}ASVC_{45}$  in *P. aerogenes*, but the other linking peptide,  $C_{20}PVDC_{24}$ , corresponds to the *P. aerogenes* sequence  $C_{18}PVNI$  following the second 4Fe center. Both molecules form antiparallel  $\beta$ -structure loops around 4Fe centers:  $C_{24}-C_{39}$  in *A. vinelandii* and  $C_{18}-C_{35}$  in *P. aerogenes*.

With 107 amino acids, *Azotobacter* ferredoxin is considerably larger than *P. aerogenes* ferredoxin (54 residues) and HiPIP (85 residues). The extra protein may serve to further insulate the 4Fe center. Four of the six basic residues adjacent to the 3Fe center (K98, K100, H103, and R106) are provided by the COOH terminus, and these could play a role in stabilizing the low potential center or as a recognition site.

**The 4Fe Center.**—The formation of a [4Fe-4S] cluster in this molecule is governed by the same rule as in *P. aerogenes* ferredoxin (12): a triplet of cysteine residues ( $n, n + 3, n + 6$ ) plus one cysteine distal in the sequence.

The paradox presented by the 4Fe center in this structure is that it is similar in character to HiPIP, but the sequence forming the center is homologous to a clostridial ferredoxin. What factors determine the oxidation-reduction potential? In keeping with the "three-state hypothesis" (46) and the EPR data (5), the geometry of the [4Fe-4S] core in the reduced or isolated state of the protein would be expected to agree best with data from reduced HiPIP crystals (15) and oxidized *P. aerogenes* ferredoxin (13). In addition,  $NH \cdots S_\gamma$  hydrogen bonds about the cluster should be more like those in HiPIP

than in *P. aerogenes* ferredoxin (41).

In the absence of a fully refined structure, accurate comparisons concerning the [4Fe-4S] core geometry cannot be made. However, comparisons can be made at a more basic level of the structure. If one views the 4Fe center down the  $S_\gamma(24)$  to Fe1 bond, the handedness of the triplet of ligands,  $S_\gamma(39) \cdots S_\gamma(42) \cdots S_\gamma(45)$  is counter-clockwise. Taking the same view from  $C_{18}$  or  $C_{45}$ , the unique cysteines in the 4Fe centers in *P. aerogenes* ferredoxin, the ligand triplets are clockwise. Thus, the polypeptide chain enfolds the [4Fe-4S] cluster in *Azotobacter* ferredoxin in a completely different manner. This must be a consequence of the 3Fe center in the  $NH_2$ -terminal portion of the molecule. The sequence  $C_{20}PVDC_{24}$  is involved in linking the two centers rather than initiating the  $\beta$ -loop; V17 and V19 of the 3Fe peptide interact with A53 and F55, respectively, near the 4Fe center. The environment of the cluster also includes two aromatic amino acids, F25 and F55. However, F2 is more than 20 Å from the 4Fe center, whereas in *P. aerogenes* the corresponding residue, Y2, interacts with the second 4Fe center. The  $\beta$ -loop between  $C_{24}$  and  $C_{39}$  is directed away from the 3Fe center; in *P. aerogenes* this loop (including Y28) lies adjacent to the first 4Fe center in the sequence.

Carter has defined a unique stereochemical orientation for [4Fe-4S] clusters based on correlations between the structures of HiPIP and *P. aerogenes* ferredoxin (47). If comparison is made solely on the basis of the  $C_{24}-C_{39}$   $\beta$ -loop and the analogous loops in the other two structures, then the unique orientation, defined by  $S_\gamma(42)$ , has the opposite hand for the direction of the polypeptide chain and observed cysteine connections. If  $S_\gamma(24)$  is chosen to define the unique orientation instead, then F25 stacks on the same face of the cluster (containing  $Fe-S_\gamma(24) \cdots Fe-S_\gamma(42)$ ) as Y19 in HiPIP. The interaction of the second aromatic residue F55, on the face of the cluster containing  $Fe-S_\gamma(39)$  and  $Fe-S_\gamma(45)$ , has no precedent in *P. aerogenes* ferredoxin or HiPIP.

**Acknowledgments.**—K. Melis is thanked for expert technical assistance in the preparation of ferredoxin and growth of crystals. Dr. A. Robbins is thanked for many stimulating discussions.

**Note Added in Proof.**—Refinement of the structure has been carried out at 2.0 Å resolution.  $R$  is 0.249 for 856 protein atoms and 327 solvent molecules with 6249 reflections at 6.0  $\sigma(|F|)$  in the range 10.0–2.0 Å. The root mean square deviation from ideality of 2406 interatomic distances is 0.025 Å.

Refinement at 2.0 Å has led to an increasingly clear image of the [3Fe-3S] cluster. In particular, electron density at the fourth coordination position of Fe(2) has resolved from the main chain electron density and weaker electron density for the E18 side chain has developed in the cleft; the density of adjacent residues 16, 17, 19, and 20 is well defined, as is that for the main chain atoms of residue 18. The peak proximal to Fe(2) has the same electron density as tightly bound water ( $1.4 e^-/\text{\AA}^3$ ) and refines to  $B = 13 \text{ \AA}^2$ , the same thermal factor of the [3Fe-3S] cluster atoms. The  $B$  values of the E18 side chain atoms are 25–27  $\text{\AA}^2$ . The data are not inconsistent with the presence of a water molecule (or hydroxyl) bound to Fe(2). Alternatively, the E18 side chain is disordered between two or more conformations, since the nonbound conformation of E18 requires rotations about  $C_\alpha-C_\beta$  and  $C_\beta-C_\gamma$  only. In either case, it appears that E18 may play an important role in the chemistry of this [3Fe-3S] cluster.

## REFERENCES

1. Shethna, Y. I. (1970) *Biochim. Biophys. Acta* **205**, 58–62
2. Yoch, D. C., Benemann, J. R., Valentine, R. C., and Arnon, D. I. (1969) *Proc. Natl. Acad. Sci.* **64**, 1404–1410
3. Yoch, D. C., and Arnon, D. I. (1972) *J. Biol. Chem.* **247**, 4514–4520
4. Yoch, D. C., and Carithers, R. P. (1978) *J. Bacteriol.* **136**, 882–824
5. Sweeney, W. V., Yoch, D. C., and Rabinowitz, J. C. (1975) *J. Biol.*



- Chem.* **250**, 7842-7847
6. Averill, B. A., Bale, J. R., and Orme-Johnson, W. H. (1978) *J. Am. Chem. Soc.* **100**, 3034-3043
  7. Emptage, M. H., Kent, T. A., Huynh, B. H., Rawlings, J., Orme-Johnson, W. H., and Münck, E. (1980) *J. Biol. Chem.* **255**, 1793-1796
  8. Huynh, B. H., Moura, J. J. G., Moura, I., Kent, T. A., LeGall, J., Xavier, A. V., and Münck, E. (1980) *J. Biol. Chem.* **255**, 3242-3244
  9. Kent, T. A., Huynh, B. H., and Münck, E. (1980) *Proc. Natl. Acad. Sci.* **77**, 6574-6576
  10. Howard, J. B., Lorschach, T., and Que, L. (1976) *Biochem. Biophys. Res. Commun.* **70**, 582-588
  11. Tsunoda, J. N., Yasunobu, K. T., and Whiteley, H. R. (1968) *J. Biol. Chem.* **243**, 6262-6272
  12. Adman, E. T., Sieker, L. C., and Jensen, L. H. (1973) *J. Biol. Chem.* **248**, 3987-3996
  13. Adman, E. T., Sieker, L. C., and Jensen, L. H. (1976) *J. Biol. Chem.* **251**, 3801-3806
  14. Carter, C. W., Jr., Kraut, J., Freer, S. T., Xuong, N., Alden, R. A., and Bartsch, R. G. (1974) *J. Biol. Chem.* **249**, 4212-4225
  15. Carter, C. W., Jr., Kraut, J., Freer, S. T., and Alden, R. A. (1974) *J. Biol. Chem.* **249**, 6339-6346
  16. Freer, S. T., Alden, R. A., Carter, C. W., Jr., and Kraut, J. (1975) *J. Biol. Chem.* **250**, 46-54
  17. Fukuyama, K., Hase, T., Matsumoto, S., Tsukihara, T., Katsube, Y., Tanaka, N., Kakudo, M., Wada, K., and Matsubara, H. (1980) *Nature* **286**, 522-524
  18. Watenpaugh, K. D., Sieker, L. C., and Jensen, L. H. (1979) *J. Mol. Biol.* **131**, 509-522
  19. Adman, E. T., Sieker, L. C., Jensen, L. H., Bruschi, M., and LeGall, J. (1977) *J. Mol. Biol.* **112**, 113-120
  20. Stout, C. D. (1979) *J. Biol. Chem.* **254**, 3598-3599
  21. Stout, C. D. (1979) *Nature* **279**, 83-84
  22. Stout, C. D., Ghosh, D., Pattabhi, V., and Robbins, A. H. (1980) *J. Biol. Chem.* **255**, 1797-1800
  23. Strahs, G., and Kraut, J. (1968) *J. Mol. Biol.* **35**, 503-512
  24. Dickerson, R. E., Kopka, M. L., Varum, J. C., and Weinzierl, J. E. (1967) *Acta Crystallogr.* **23**, 511-522
  25. Petsko, G. A., Phillips, D. C., Williams, R. J. P., and Wilson, J. A. (1978) *J. Mol. Biol.* **120**, 345-359
  26. Dickerson, R. E., Kendrew, J. C., and Strandberg, B. E. (1961) *Acta Crystallogr.* **14**, 1188-1195
  27. Hase, T., Wakabayashi, S., Matsubara, H., Ohmori, D., and Suzuki, K. (1978) *FEBS Lett.* **91**, 315-319
  28. Konnert, J. H. (1976) *Acta Crystallogr.* **A32**, 614-617
  29. Furey, W., Wang, B. C., and Sax, M. (1980) Abstracts of the American Crystallographic Association Summer Meeting, Calgary, Canada, p. 27 (abstract G1)
  30. Holm, R. H., and Ibers, J. A. (1977) in *Iron-Sulfur Proteins* (Lovenberg, W., ed) Vol. III, pp. 205-281, Academic Press, New York
  31. Menzebach, G., and Bleckman, P. (1975) *J. Organometallic Chem.* **91**, 291-294
  32. Kraut, J., Strahs, G., and Freer, S. T. (1968) in *Structural Chemistry and Molecular Biology* (Rich, A., and Davidson, N., eds) pp. 55-64, W.H. Freeman, San Francisco
  33. Stanford, R. H. (1964) *Acta Crystallogr.* **17**, 1180-1181
  34. Matsubara, H., Sasaki, R. M., Tsuchiya, D. K., and Evans, M. C. W. (1970) *J. Biol. Chem.* **245**, 2121-2131
  35. Hase, T., Matsubara, H., and Evans, M. C. W. (1977) *J. Biochem.* **81**, 1745-1749
  36. Bruschi, M., Bovier-Lapierre, G., Bonicel, J., and Couchoud, P. (1979) *Biochem. Biophys. Res. Commun.* **91**, 623-628
  37. Hatchikian, C. E., Jones, H. E., Bruschi, M., Bovier-Lapierre, G., Bonicel, J., Couchoud, P., and Forget, N. (1979) *Biochim. Biophys. Acta* **548**, 471-483
  38. Hase, T., Wakabayashi, S., Matsubara, H., Imai, T., Matsumoto, T., and Tobari, J. (1979) *FEBS Lett.* **103**, 224-228
  39. Moss, T. H., Bearden, A. J., Bartsch, R. G., Cusanovich, M. A., and San Pietro, A. (1968) *Biochemistry* **7**, 1591-1596
  40. Ohnishi, T., Blum, H., Sato, S., Nakazawa, K., Hon-nami, K., and Oshima, T. (1980) *J. Biol. Chem.* **255**, 345-348
  41. Adman, E., Watenpaugh, K. D., and Jensen, L. H. (1975) *Proc. Natl. Acad. Sci.* **72**, 4854-4858
  42. Kurtz, D. M., Holm, R. H., Ruzicka, F. J., Beinert, H., Coles, C. J., and Singer, T. P. (1979) *J. Biol. Chem.* **254**, 4967-4969
  43. Yoch, D. C., Carithers, R. P., and Arnon, D. I. (1977) *J. Biol. Chem.* **252**, 7453-7460
  44. Berndt, H., Lowe, D. J., and Yates, M. G. (1978) *Eur. J. Biochem.* **86**, 133-142
  45. Yates, M. G., O'Donnell, M. J., Lowe, D. J., and Bothe, H. (1978) *Eur. J. Biochem.* **85**, 291-299
  46. Carter, C. W., Kraut, J., Freer, S. T., Alden, R. A., Sieker, L. C., Adman, E., and Jensen, L. H. (1972) *Proc. Natl. Acad. Sci.* **69**, 3526-3529
  47. Carter, C. W., Jr. (1977) *J. Biol. Chem.* **252**, 7802-7811
  48. Miller, J. R., Abdel-Mequid, S. S., Rossmann, M. G., and Anderson, D. C., (1981) *J. Appl. Crystallog.*, in press